Journal of Civil Engineering and Construction 2023;12(3):126-141
https://doi.org/10.32732/jcec.2023.12.3.126

Modelling of Inelastic Pentamode-Based Bridge Bearings Using Beam Elements

Olga E. Sapountzaki[1], Andreas E. Kampitsis[2], Nikos D. Lagaros[1]

1. Institute of Structural Analysis & Antiseismic Research, Department of Structural Engineering, School of Civil Engineering, National Technical University of Athens, Iroon Polytechniou Str. 9, Zografou Campus, GR-15780 Athens, Greece
2. Institute of Structural Analysis & Dynamics of Structures, School of Civil Engineering, Aristotle University of Thessaloniki, 54124 Thessaloniki, Greece
E-mail: olgasapountzaki@central.ntua.gr; cvakamb@gmail.com; nlagaros@central.ntua.gr

Received: 23 January 2023; Accepted: 23 May 2023; Available online: 1 August 2023

Abstract: Metameterials have unique properties, which are mostly attributed to their geometrical configuration. Pentamodes, a subcategory of metamaterials, exhibit an almost zero shear elastic modulus while maintaining high compression stiffness, offering a behavior similar to that of a liquid, suggesting the potential application of pentamodes in seismic isolation. In this paper a real-life bridge bearing, composed of repetitive layers of pentamode unit cells in the horizontal and vertical axes is studied. The lattices are modelled using beam finite elements with an equivalent uniform diameter to ensuring a stiffness equal to that of the bi-cone rod. The importance of the chosen equivalent diameter is shown, as the assumption of an average diameter of the bi-cone may lead to significant discrepancies between the calculated stiffnesses. For small bi-cone diameters difference, and slender formulations, the error could grow up to 15% for the horizontal stiffness and up to 200% for vertical. For thick formulations the average diameter overestimates the horizontal stiffness by 3 times and the vertical by 4. These discrepancies grow exponentially as the bi-cone diameters difference increases. An elastoplastic material is selected. The bearing supporting the superstructure is subjected to a constant vertical weight load and a horizontal shear base load, due to seismic excitation. Under vertical loading plastic hinges are created in all the rods of the cell and bearing. However, under shear loading plastic hinges are rather initially created in the lowest nodes of the cell and the bearing.
Keywords: Pentamode lattices; Equivalent diameter; Bridge bearing; Inelastic response; Failure mechanisms.

1. Introduction

Over the last years, new materials with unconventional properties have been extensively investigated. Amongst them, metamaterials have drawn the attention of the research community. Their advanced mechanical properties have resulted in major interest in numerous fields, including space, aeronautic, mechanical and civil engineering with potential use for the development of spacecraft parts, aircraft wings, wind turbine blades, uncracked materials, and bridge bearings. The tailor-made properties of the metamaterials are mainly attributed to their internal structural topology rather than the unique chemical composition of the comprising materials. An example of metamaterials combining both a negative mass and a negative bulk modulus was proposed by Liu et al [1]. The double negative value properties were obtained by utilizing simultaneously the local translational and rotational resonances of a chiral microstructure.

A promising field of metamaterials is that of the pentamodes. Pentamode materials are formulated by repeating lattices of unit cell comprised of four beamlike elements intersecting at a central point. The pentamode formulation has been proved to feature five zero-energy deformation modes, namely five soft deformation modes, and a single non-zero, i.e., stiff deformation mode. This implies that the eigenvalues corresponding to the five soft ones are almost equal to zero. They appear to be exhibiting a high elasticity modulus. Despite being solid, their behavior assimilates more the one of fluid materials with an almost zero shear modulus. Hence, the idea of pentamodes being applied to the damping of shear waves sounds really fascinating and leads to the discussion of the plausibility of their application in seismic isolation.

Seismic isolation is a field, which has gained a lot of attraction in the past decades. Many novelties have been proposed for application, since the need to ensure an efficient and cost-effective damping system concerns a great part of the world. Except for pentamodes, negative stiffness absorbers have also been discussed for the mitigation

of vibrations [2], where the authors suggested the application of the KDamper, a seismic isolation device equipped with negative stiffness elements in wind turbines.

Current literature is focused on the formulations of the pentamode internal structure as well as their applications in seismic isolation, acoustic cloaking, and frequency band gaps ([3], [4] and [5]). Milton and Cherkaev [6] proved that any given positive elasticity matrix can be realized. The unimode, bimode, up to pentamode materials with one, two and five modes, respectively equal to zero were introduced. The structure for pentamodes, which would constitute the basis of the investigation of studies to follow, was proposed. Inspired by this work, Kadic et al. [7] investigated the feasibility of such a pentamode structure. Employing the double cones formulation, the authors presented the range of bulk to shear moduli ratio, highlighting the nature of the pentamode material.

Research has also been made towards ways of designing, optimizing and producing pentamode crystals. Lumpe and Stankovic [8] investigated numerous pentamode structures showing the importance of crystallographic symmetries on the mechanical properties of the structure. Xu et al [9] proposed two different methodologies to design lattice structures with controlled anisotropy. Huang et al. [10] introduced a new class of pentamode metamaterial with centrosymmetry, showing better mechanical characteristics. Li et al [11] proposed a mathematical formulation for deriving pentamode structures with at least orthotropic symmetry. and presented various new isotropic, transverse isotropic and orthotropic lattices. Moreover, Wu et al [12] designed various pentamode structures using topological optimization to achieve a high, yet realistic, bulk modulus. The influence of the geometrical characteristics on the effective properties was shown.

Various crystals were designed by Fabroccino et al. [13] using tensegrity architecture, which can exhibit significant advantages compared to conventional seismic rubber bearings, such as the ability to be adjusted to the targeted structure and the freedom to choose among a variety of available materials to ensure the desired properties. The proposed formulations offer high-energy dissipation. The replacement of the vibration absorbing parts of the bearing with pentamode materials was proposed. The advantages of pentamode lattices compared to conventional seismic bearings were analyzed by Fraternali et al. [14]. Their mechanical properties were numerically investigated with respect to their geometrical arrangement and applications in seismic isolation were illustrated.

Amendola et al. [15] proposed a variation in the pentamode lattices, which in the horizontal axis is constituted of two primitive cells and in the vertical axis is stiffened using confinement plates. The authors studied experimentally the response in the elastic and post – yield domain and proved that it is dominantly bending. The influence of the confinement plates on the shear and bulk modulus was analyzed, highlighting how the geometry of such arrangements can influence the properties of the pentamode. It was concluded that such lattices could be applied in vibration absorption, due to their high-energy dissipation in the post – elastic region. The properties of the pentamode formulations were also investigated numerically by Amendola et al. [16]. A comparison between unconfined and lattices confined by stiffening plates was made. In the first case, shear and elastic modulus were quite similar; in contrast to the near zero shear modulus of confined lattices. The similarity between the pentamode lattices and the elastomeric bearings, suggested the potential to be used in seismic isolation applications.

Fraternali and Amendola [17] studied a pentamode formulation where the unit cell was formed by two primitive cells instead of four. The authors proved that this formulation had three soft modes instead of five, with effective compression modulus being equal to the two thirds of the elastic modulus of the stiffest elastic formulation. Further, Amendola et al. [18] studied the response of the above pentamode under large elastic strain presenting the elastic – stiffening effect. The proposed pentamode response was also shown to be influenced by the nodes´ rigidity and the number of the confinement plates. In both papers the pentamode application in bearings was underlined.

In this work, a bridge bearing composed of layered pentamode modules, is studied. The bearing is constructed by repetitive layers of pentamode unit cells in both the horizontal and vertical axes. A pentamode module is comprised of pentamode unit cells and each cell of intersecting bi-cone rods. The novelty of this research is the use of a homogeneous elastoplastic material to simulate the nonlinear inelastic response of the rods. The bearing is subjected to a constant vertical load due to the weight of the superstructure as well as to a horizontal shear base load, due to seismic excitation. Plastic hinges are created overall on the formulation level under vertical loading, whereas under shear loading the plastic hinges are mostly created on the lowest nodes of the cells It is concluded that the bearing features enough shear and compression stiffness to withstand the real-scale induced shear base and can thus be characterized as seismic-isolation device.

The pentamode bi-cone rods are modelled via beam finite elements with an equivalent uniform diameter. The equivalent diameter is calibrated as such to provide the same bending and shear stiffness equal to that of the bi-cone rod. For the first time in literature, it is shown that the stiffness obtained by using the average of the large and small diameter of the bi-cone rod does not always accurately represent the real stiffness parameters of the pentamode structure. The assumption of an average diameter of the bi-cone leads to a significant discrepancy between the calculated stiffnesses. For small bi-cone diameters difference, and for slender formulations, the error could grow up to 15% for the horizontal stiffness and up to 200% for vertical. Similarly, for thick formulations the average D overestimates the horizontal stiffness by 3 times and the vertical one by 4 times. These discrepancies

grow exponentially as the bi-cone diameters difference increase, leading to an unsafe modelling assumption. The equivalent diameter for a pentamode formulation must be chosen according to the geometry of the crystal.

2. Modelling of pentamode lattices

2.1 Equivalent diameter of a cellular structure

A pentamode module is constructed by four pentamode unit cells and each cell by four (Z=4) beam-like elements. The shape of the unit cell is the truncated double cone, as shown in Figure 1. The ends of all the elements are fixed at their geometric center. The pentamode elements are attributed bending stiffness in addition to their axial rigidity. In other words, in the numerical formulation each unit cell is modelled using four beam finite elements. This formulation is shown in Figure 2a. Four unit cells constitute a pentamode module, as shown in Figure 2b.

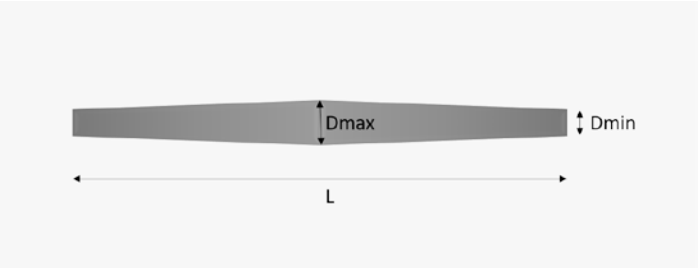

Figure 1. Maximum and minimum diameter of the bi-cone lattice.

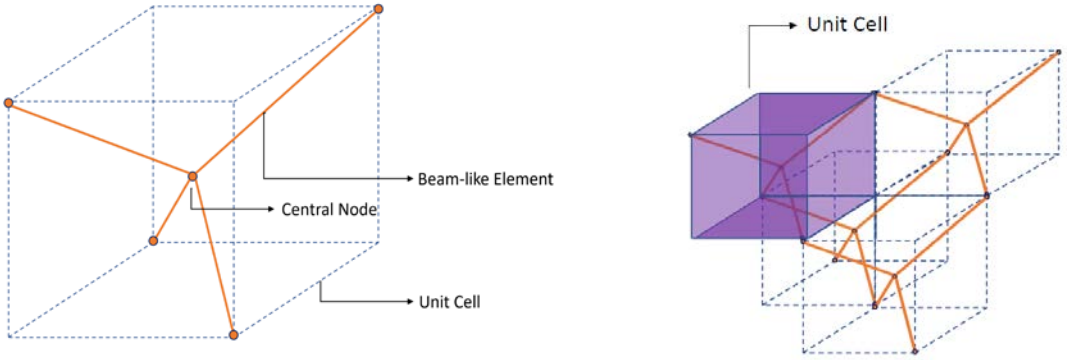

(a) (b)

Figure 2. Pentamode unit cell composed of four beam elements (a) and pentamode module composed of 4 unit cells (b).

Pentamodes, offer applications in many fields. However, in order to be applicable, the design, the simulation, and the analyses of the pentamode structures need to be cost- and time-effective. 3D solid elements offer higher precision and enable a simulation with truncated double cones, but such a sophisticated modelling is highly computational demanding. Thus, it is strongly suggested that pentamode structures are simulated using beam elements, utilizing the computational efficiency and the accuracy of such modelling approach.

Subsequently, the question that arises is: "What is the equivalent uniform diameter of the beam element to accurately model the double cone lattice of the pentamode cell?". In most of the existing studies, the average of the two diameters of the bi-cone is used. However, that simplification does not ensure the match between the bending and shear stiffness of the beam element to that of the bi-cone rod. Herein, an equivalent uniform diameter is proposed that accurately represents both the bending and the shear stiffness of the actual rod. To this end, the equivalent diameter is calibrated against experimental results from previous studies.

2.2 Formulation and verification for elastic material

Let us first consider a pentamode unit cell in the elastic region. The bending stiffness, and the ratio of shear to bending stiffness of the unit [14] are given in Eqs. (1) and (2):

$$K = 4R^2/9MV \quad (1)$$

$$G/K = 9M/(4M + 2N) \quad (2)$$

where R is the lattice´s length; M and N are the bending and axial compliance given in Eqs. (3) and (4).

$$M_i = \int_0^{Ri} dx/E_iA_i, \quad (3)$$

$$N_i = \int_0^{Ri} x^2 dx/E_iI_i \quad (4)$$

Following the study of Amendola et al [15], two kinds of crystals are studied, namely the slender and the thick pentamode specimens (SPMs and TPMs). The base of the SPMs is composed of 2×2 pentamode modules and its height is four pentamode modules. Thus, its geometry can be described as 2×2×4. Similarly, the TPM base is composed of 2×2 pentamode modules, while its height is two pentamode modules, i.e., 2×2×2.

As shown in Figure 1, the double cone mid diameter (D), is the largest diameter of the rod and is equal for all the crystals. The end-point diameter of the rod is the smallest one (d) and dictated the connection forces between the inter-joining rods. Three types of end-point diameters (d) are examined in this study. The sets of the large and small diameters are shown in Table 1.

Table 1. Sets of small & great diameters used for TPMs & SPMs

d (*mm*)	D (*mm*)
0.49	2.72
1.04	
1.43	

The length R of the rods is considered the same in all cases examined. The rods are composed of homogeneous, isotropic titanium alloy with elasticity modulus of E = 120GPa and Poisson ration of v = 0.3. The alloy is described as elastic - perfectly plastic and its behavior can be described by the stress-strain curves as shown in Figure 3. In the current study all the specimens are modelled in Abaqus/ CAE 6.9-1 software [19]. For the 3D configuration of the pentamode unit cell, the rods are modelled using beam Finite Elements (FE) with constant circular cross section. The inter-joining elements are assumed to be linked with fixed connections at the common nodes, while diaphragms with kinematic coupling are utilized to simulate the imposed deformation restrains.

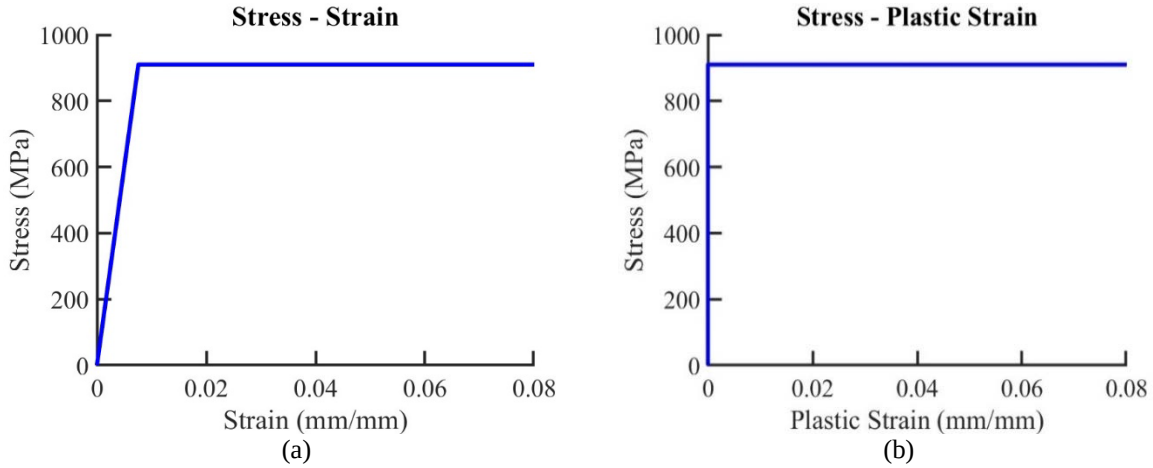

Figure 3. Stress-strain (a) & Stress-plastic strain (b) curves for the titanium alloy.

The equivalent diameter of the FE circular cross section is expressed as a linear function of the larger (D) and smaller (d) diameters of the specimen, provided that the sum of the two coefficients is equal to one, i.e. can be described by Eq. (5):

$$d_{eq} = a_1 \times D + a_2 \times d, \text{ where } a_1 + a_2 = 1 \quad (5)$$

A unique equivalent diameter is identified for each one of the six crystals under investigation. Note that the diameter coefficients for the SPMs might show great deviation from that of the TPMs. The reason can be found in the difference of the response of the two specimens. In the TPMs case, the response can be characterized as shear – dominated, whereas in the SPMs case the response is mainly bending. Therefore, the accurate calculation of the equivalent diameter plays a crucial role, especially in the case of a thick specimen. The slender crystals show high values of horizontal displacements regardless of the diameter. The above findings are depicted in Figure 4 (a), where the variation of the horizontal stiffness is shown as a function of the equivalent rod diameter. In this graph

the horizontal stiffness for the TPMs and SPMs as a function of the equivalent diameter of the rod is plotted (blue curve for the TPMs and red curve for the SPMs). Moreover, the results for the small and large diameters (Table 1) are marked with asterisks (yellow asterisks for the TPMs and blue asterisks for the SPMs), showing the minimum and maximum possible stiffness, that the specimens may feature. Squares (red for the TPMs and magenta for the SPMs) are used to mark the stiffness that would be obtained, if the equivalent diameter would be computed as the average of the small and the large diameter. Subjecting all SPMs and TPMs specimens to horizontal loading and calibrating the findings with the experimental results by Amendola et al [15], Eqs. (6) and (7) can be suggested for the equivalent diameter for SPMs and TPMs respectively:

$$d_{eq} = 0.28 \times D + 0.72 \times d \quad (6)$$

$$d_{eq} = 0.17 \times D + 0.83 \times d \quad (7)$$

The results that are obtained for the equivalent diameters according to Eqs. (6) and (7) are marked in Figure 4 using dots (green for the TPMs and navy for the SPMs). The error between the results obtained by the average of the small and the large diameter and the results obtained by using the suggested equations is also shown on the graphs. Additionally, it is calculated and listed alongside with the obtained stiffnesses in Table 2.

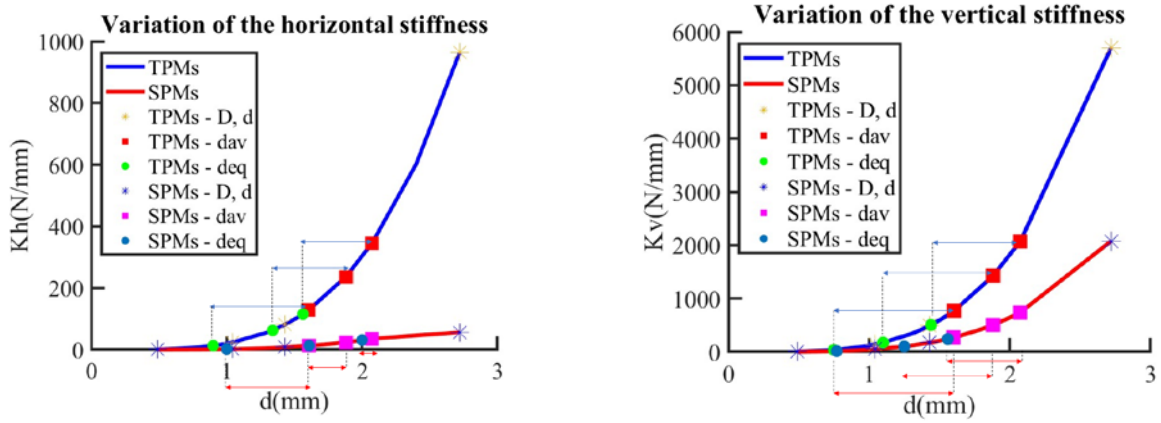

(a) (b)

Figure 4. Variation of the horizontal (a) and vertical (b) stiffness of the TPMs & SPMs as a function of the equivalent diameter.

Table 2. Diameters, Stiffnesses & Calculated Errors for the horizontal stiffness

Specimen	D (mm)	d(mm)	d_{av}(mm)	$K_{dav,Abaqus}$ (N/mm)	deq(mm)	$K_{exp} = K_{deq,Abaqus}$ (N/mm)	Calculated Error (%)
TPM1	2.72	0.49	1.605	128.21	0.90	13.10	878.6
TPM2	2.72	1.04	1.88	236.59	1.34	63.16	274.6
TPM3	2.72	1.43	2.075	346.02	1.56	115.74	198.9
SPM1	2.72	0.49	1.605	13.18	1.00	2.00	557.3
SPM2	2.72	1.04	1.88	24.18	1.61	13.18	84.6
SPM3	2.72	1.43	2.075	35.5	2.00	30.79	15.3

The same process was followed for the vertical loading. In Figure 4 (b) the variation of the vertical stiffness as a function of the equivalent diameter, are presented. The same symbols were used to show the findings for the vertical stiffness.

It is worth mentioning that the horizontal and vertical stiffness of both the TPMs and the SPMs should be expressed with a different equation. Thus, for the vertical stiffness Eqs. (8) and (9) can be suggested for the equivalent diameter for SPMs and TPMs respectively:

$$d_{eq} = 0.12 \times D + 0.88 \times d \quad (8)$$

$$d_{eq} = 0.09 \times D + 0.91 \times d \quad (9)$$

Similarities can be found between the response to the horizontal and the vertical loading. Once again, the thicker specimens seem to be strongly influenced by the variation of the diameters of the beams. The vertical stiffness is

however stronger influenced by the diameter than the horizontal stiffness. The reason is that in the case of lateral loading (especially in the thin specimens, but to some extent also in the thick ones) the bending is an important part of the displacement. The error between the results with the equivalent diameter, as this is suggested in the current paper, and the average of the large and small diameter is large especially for the TPMs. It seems however, that the slenderer the specimen, the lower this error is. Similarly, the lower the difference between the large and the small diameter, the lower the error.

Table 3. Diameters, Stiffnesses & Calculated Errors for the vertical stiffness

Specimen	D(mm)	d(mm)	d_{av}(mm)	$K_{dav,Abaqus}$ (N/mm)	deq(mm)	$K_{exp} = K_{deq,Abaqus}$ (N/mm)	Calculated Error (%)
TPM1	2.72	0.49	1.605	771.01	0.75	38.46	1904.6
TPM2	2.72	1.04	1.88	1421.67	1.10	175.22	711.3
TPM3	2.72	1.43	2.075	2075.12	2.08	505.05	310.9
SPM1	2.72	0.49	1.605	268.38	0.77	14.84	1708.4
SPM2	2.72	1.04	1.88	503.78	1.25	101.52	396.2
SPM3	2.72	1.43	2.075	739.10	1.56	242.95	204.2

To generalize the behavior of the specimens, let us consider a “thicker” specimen than the TPM, which we will call TTPM and a “slenderer” specimen than the SPM, which we will call SSPM. The TTPM has the same height as a TPM and a greater length and width, namely dimensions of 4×4×2 pentamode modules. The SSPM has the same length and width as the SPM and a height of 6 modules, namely dimensions of 2×2×6. In Figure 5 and Figure 6, the variation of the horizontal and vertical stiffness respectively for the TTPM and the SSPM in comparison to those for the TPM and the SPM is shown. Although in both cases the curves for the SPMs and the SSPMs show negligible deviation from each other (curves coinciding on the graph), the slope of the curves for the TPMs and the TTPMs vary significantly.

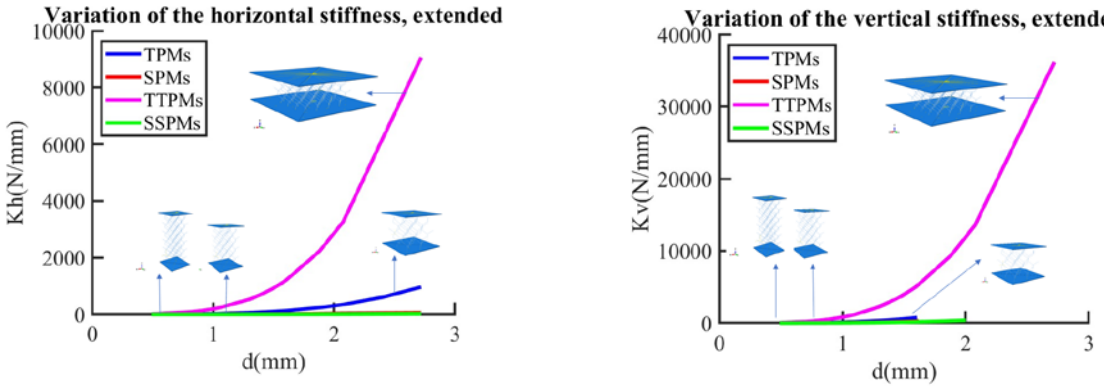

(a) (b)

Figure 5. Variation of the horizontal (a) and vertical (b) stiffness of the TTPMs & SSPMs as a function of the equivalent diameter.

To sum up the above findings, it can be stated that the diameter influences the vertical and horizontal stiffness of a pentamode formulation only in case of thick formulations. In these cases, it is crucial that the equivalent diameter would not be calculated as the average of the small and the large diameter, since that would lead in great errors. The reason is the dominantly bending response in the case of slender formulations.

2.3 Formulation and verification for elastic, perfectly plastic material

In the plastic region, the lumped plasticity theory is followed. Accordingly, the beam’s cross-section may yield when a yield criterion is fulfilled, creating a plastic hinge. In the inelastic regime, the stress field can be obtained from Eq. (10):

$$\sigma = E\varepsilon_{el} + \varepsilon_{pl} \tag{10}$$

The elastoplastic material of Figure 3 is implemented in the Abaqus FE model. Similarly, to section 2.2.1, the experimental results of Amendola et al [15] are used to verify the proposed model. In Amendola et al [15] two types of loading were considered: namely a cyclic one and a monotonic one until failure (push-over). In Figure 6,

the response of the TPMs and the SPMs under cyclic lateral loading is presented for different values of the equivalent diameter. As shown, the value of the diameter plays a crucial role for the yielding load.

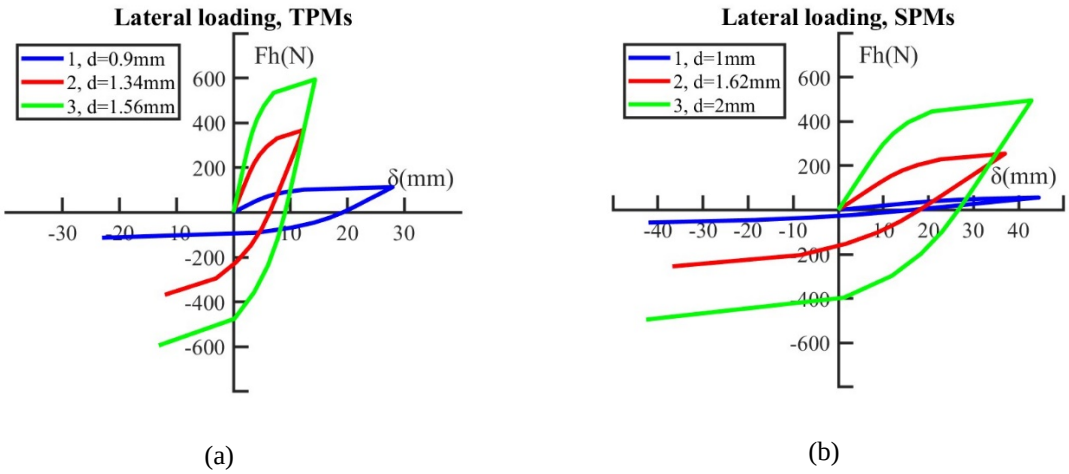

(a) (b)

Figure 6. TPMs (a) and SPMs (b) under cyclic lateral loading.

These figures once again show the impact of the equivalent diameter of the rods on the lateral stiffness of the specimens, especially in the case of the TPMs. Additionally, comparing the green curves; one can easily conclude that the TPMs obtain greater stiffness than the SPMs with a lower diameter. The same is also concluded when comparing the blue curves as well as the red ones. The dominantly bending response of the SPMs is once again illustrated. A lateral monotonic loading until failure was also applied to the SPMs. Figure 7 shows the experimental results as presented by Amendola et al [15] and the numerical results using the equivalent diameter. The results show satisfactory accuracy with deviation of less than *10%*. The deformed and undeformed shapes are depicted on the graph for comparison.

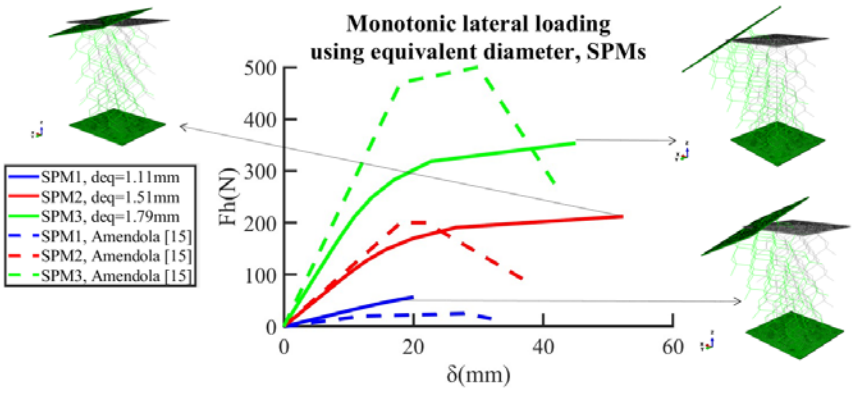

Figure 7. Comparison between experimental [15] **and the proposed numerical results.**

3. Application of pentamode lattices on bridge bearing

3.1 Nonlinear response of the pentamode unit cell

Having verified the model, we consider a pentamode unit cell, as described by Figure 2. The assumption of a constant circular cross-section with a radius of 0.99mm was maintained throughout the current example. The material of the pentamode rod is considered to follow the polymer properties with elasticity modulus E = 341MPa and Poisson ratio v = 0.3. Its behavior can be characterized as isotropic, elastic – perfectly plastic as described in Figure 8. The lower level of the unit cell is assumed to be fixed, while the top level is restrained by a diaphragm.

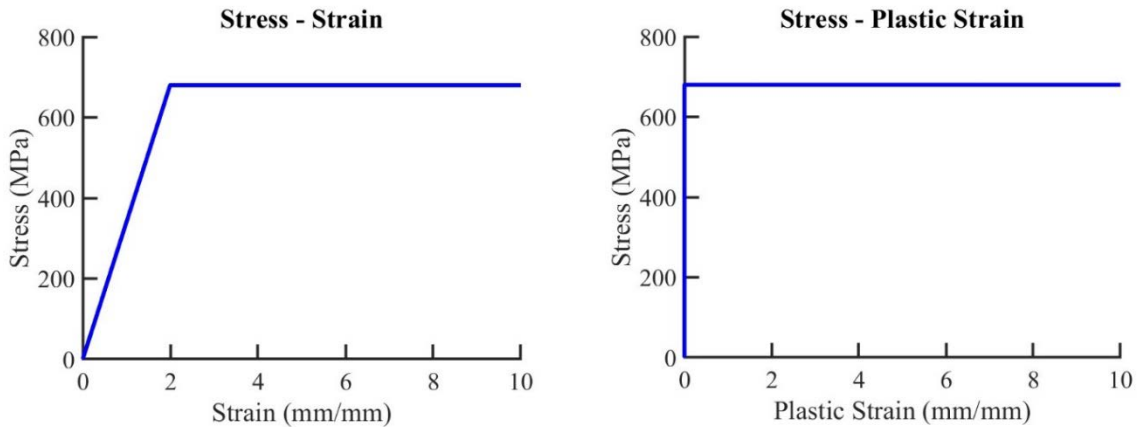

(a) (b)

Figure 8. Stress-strain (a) & Stress-plastic strain (b) curves for the polymer material.

First, the elastic response of the pentamode unit cell of Figure 2(a) is investigated. A horizontal load of 0.1kN is applied at the diaphragm's midpoint (master node). In Figure 9, the magnitude displacement contour with the deformed shape and the von Mises stress contour are shown. In Figure 10, the blue line shows the elastic load-displacement curve of the pentamode unit cell.

Subsequently, the non-linear inelastic (Figure 8) response of the pentamode unit cell is studied. In Figure 10, the red line corresponds to the inelastic load - displacement curve (lattices have entered the plastic regime). Figure 11 shows the displacement magnitude contour with the deformed shape, and the von Mises stress contour of the cell. In Figure 12, the nodes, which have reached the yield stress at the first and the last stage of the yielding, are marked in red. Both lower fixed nodes and the central one have been converted into plastic hinges and marked in green.

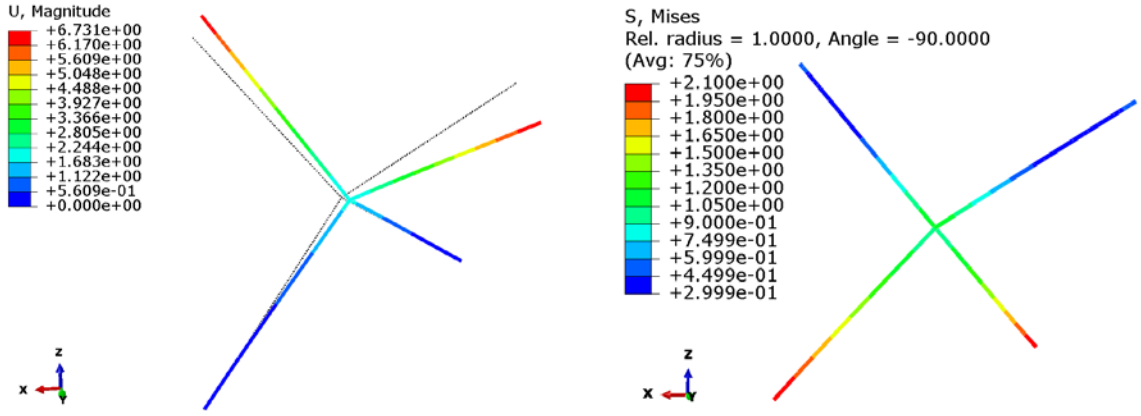

(a) (b)

Figure 9. Deformed shape & displacement contour (a) and Von Mises stress contour (b) of elastic cell under horizontal loading

The plastic hinges are first created in the lowest nodes of the cell. Next, the plastic region is extended in lower rods. After several parts of the rod have been plasticized, hinges are created in the center of the cell. Finally, the plastic region starts to extend in the rest part of the lowest nodes and in the upper nodes. These stages will constitute the key for the identification of the failure mechanisms of the pentamodes.

It is worth here mentioning that a unit cell under vertical loading is plasticized simultaneously at its upper nodes, its lower nodes and its central node. This is shown in Figure 13, where the von Mises stress contour and the plastic hinges that are first created in the cell under vertical loading are shown. The shear and compression failure mechanisms of the unit cell seem to vary from each other.

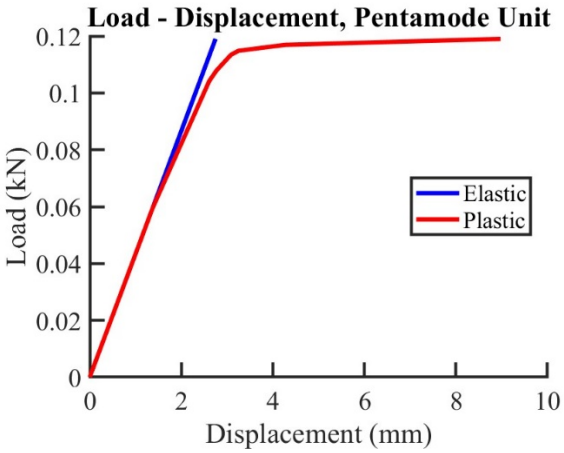

Figure 10. Load – displacement curve of elastoplastic cell under horizontal loading.

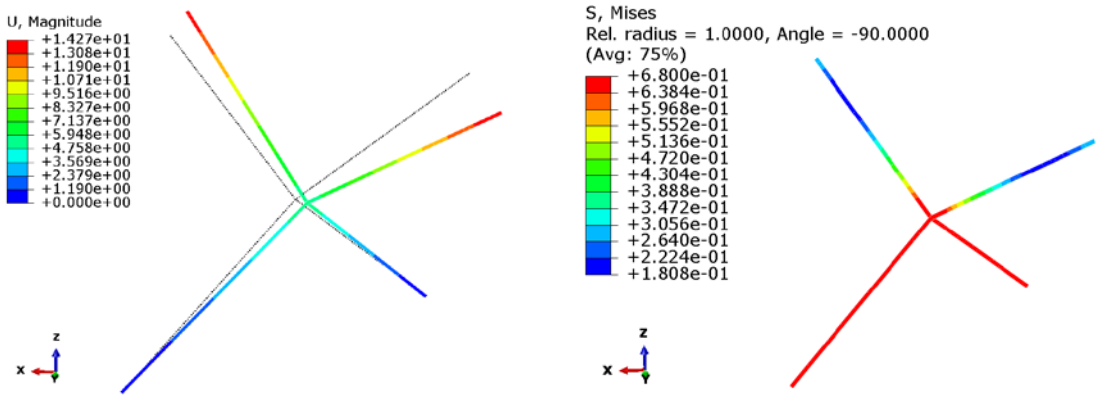

(a) (b)

Figure 11. Deformed shape & displacement contour (a) and Von Mises stress contour (b) of elastoplastic cell under horizontal loading.

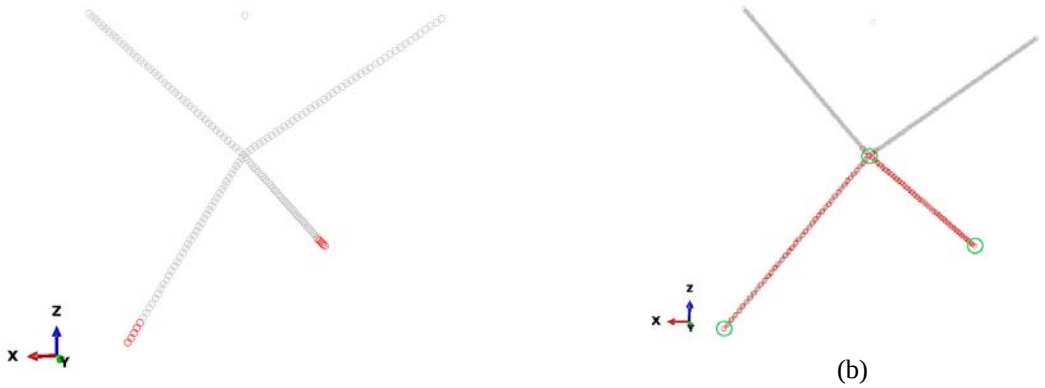

(a) (b)

Figure 12. First plastic hinges (a) and final stage of the plastic hinges (b)on the elastoplastic cell under horizontal loading.

3.2 Nonlinear response of bridge bearing pentamode lattices

Let us consider a pattern composed of vertically and horizontally connected pentamode unit cells. The formulated structure can sufficiently represent a pentamode bridge bearing. A typical bearing of dimensions 100×100mm and of height 21mm is created. On the top of the pattern, a diaphragm is applied to simulate the bridge's deck. A vertical force of 100kN is applied on its midpoint. The lower level of the bearing is fixed to the bridge´s pier. The configuration is shown in Figure 14. A closer look to a unit cell is also provided this figure.

Linear elastic analyses are performed utilizing the equivalent diameter approach. In Figure 15 the suggested configuration of the bearing, placed between the upper structure and the pier of the bridge, is depicted. Figure 16

shows the displacement magnitude contour with the deformed shape, and the von Mises stress contour. A closer look to the lowest corner of the bearing is provided to offer a better view of the contours.

Assuming that the initial condition of the structure is the compressed stage due to the superstructure weight, let us apply a horizontal displacement of 10.5mm at the diaphragm's control point. The deformed shape with the displacement contour and the von Mises stress contour are shown in Figure 17. A closer look to the same corner as before is also provided. In Figure 19, the reaction force versus the horizontal displacement is plotted.

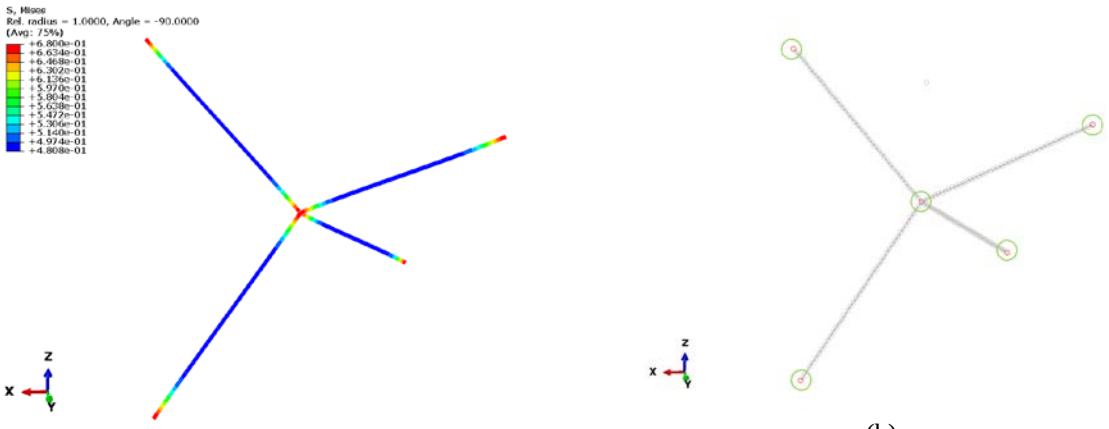

(a) (b)

Figure 13. Von Mises stress contour (a) and first plastic hinges created on the elastoplastic cell under vertical loading

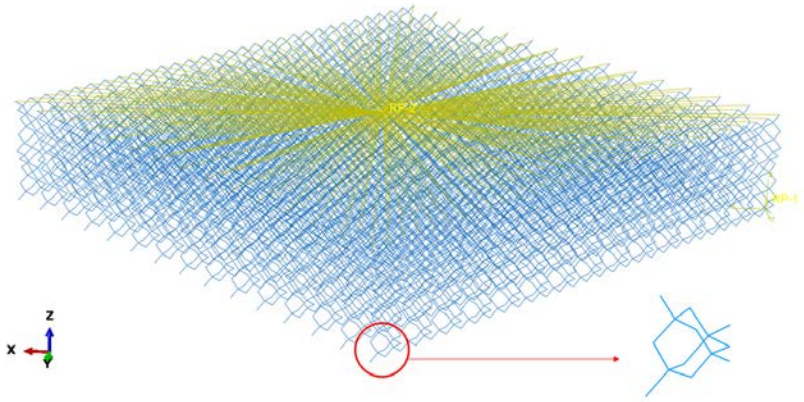

Figure 14. Formulation composed of pentamode modules and an upper diaphragm

Figure 15. Suggested arrangement for the pentamode bearing

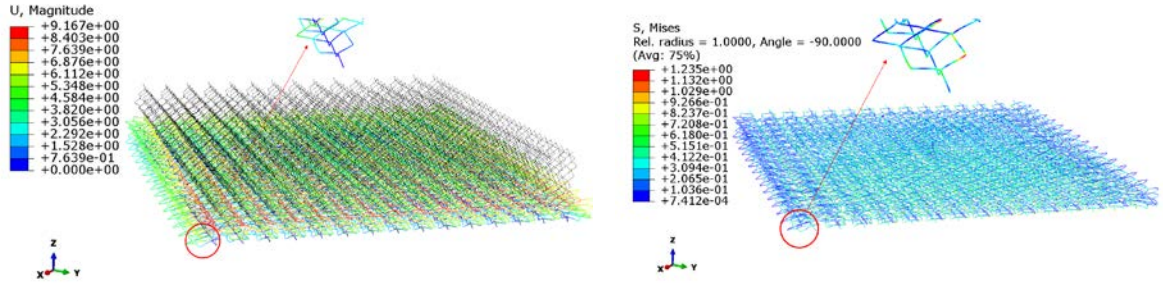

(a) (b)

Figure 16. Deformed shape & displacement contour (a) and von Mises stress contour of elastic formulation (b) under vertical loading.

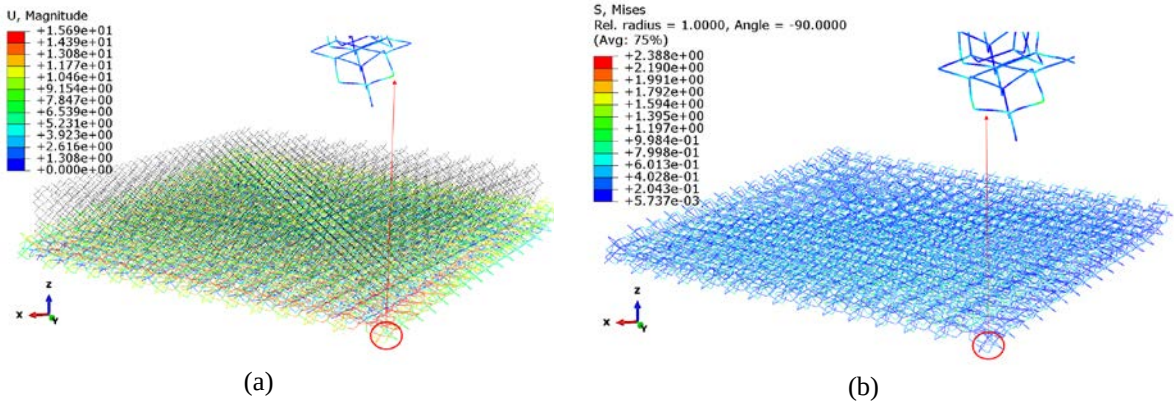

(a) (b)

Figure 17. Deformed shape & displacement contour (a) and von Mises stress contour (b) of elastic formulation under vertical loading & horizontal displacement.

3.3 Failure mechanism of bridge bearing pentamode lattices

To study the failure mechanism of the pentamode bearing, the inelastic material is assumed (Figure 8) and the bearing is simultaneously subjected under vertical loading and horizontal displacement. The deformed shape with the displacement magnitude contour and the von Mises stress contour are shown in Figure 18. A closer look to the lowest corner of the bearing is provided to offer a better view of the contours. The reaction force versus the horizontal displacement is plotted in Figure 19.

It should be mentioned that the two curves of Figure 19 have different elastic slope. The reason is that the two analyses for the horizontal force are not initiated with the same stiffness vector. As already mentioned, the horizontal force is applied after the completion of the analysis with the vertical force. Thus, plastic hinges have already been created in the elastoplastic model due to the bridge's weight. However, it is worth noting, that the slope of the plastic analysis does not seem to change significantly during the analysis.

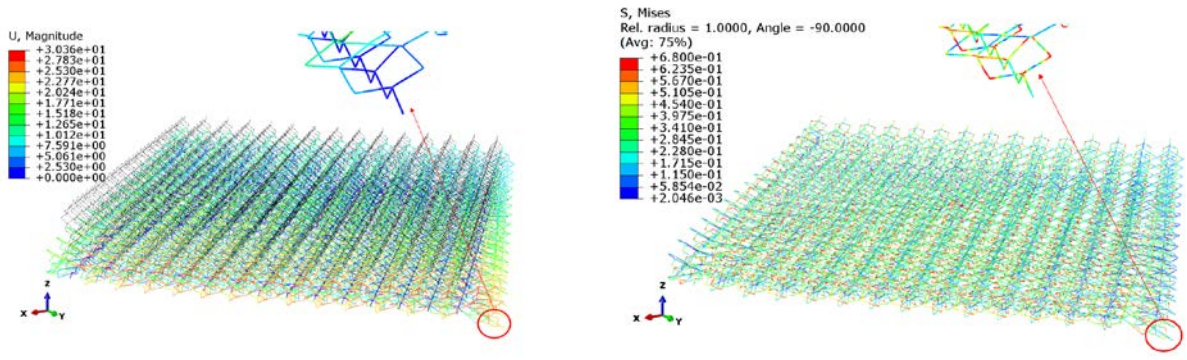

(a) (b)

Figure 18. Deformed shape & displacement contour (a) and Von Mises stress contour of elastoplastic formulation under vertical loading & horizontal displacement.

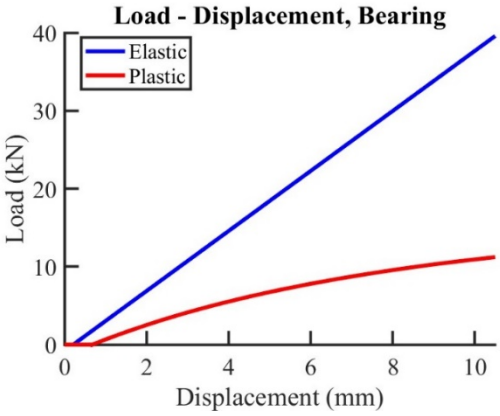

Figure 19. Reaction force –displacement curve of elastoplastic formulation under vertical loading & horizontal displacement.

Moreover, the failure mechanisms of the bearing were studied. The plastic hinges that were first created on the bearing due to the gradual application of the vertical loading are marked in red in Figure 20. The plastic hinges that were created after the application of the total vertical loading are shown in Figure 21. In Figure 22, the plastic hinges that are created to the bearing solely because of the horizontal displacement applied are shown. Final, the plastic hinges created due to the application of both the vertical loading and the horizontal displacement are shown in Figure 23. All of the Figures 20 - 23 provide a plan view of the bearing in order to show the distribution of the hinges and a closer look to the bottom corner of the bearing where the hinges are first formed.

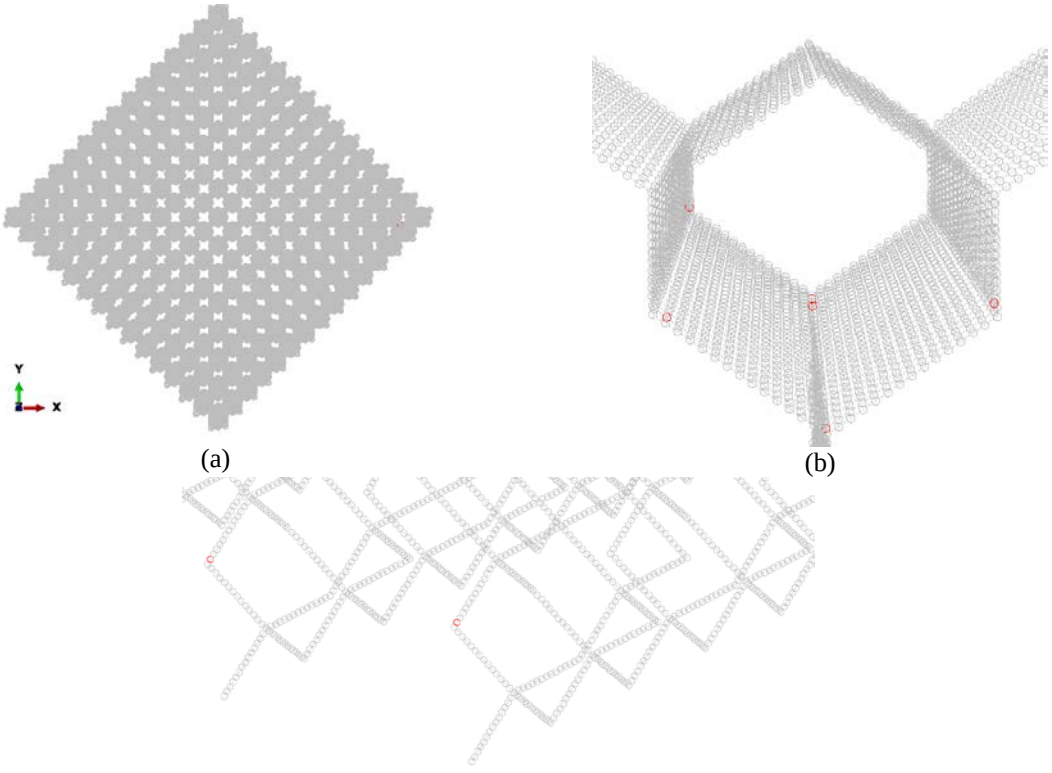

Figure 20. First plastic hinges created on the bearing due to vertical loading, (a) plan view, (b) compression failure mechanism on the top, (c) bottom corner

In the case of the vertical loading, the plastic hinges are homogeneously distributed on the bearing, since the load is applied homogeneously to the bearing via the diaphragm. It should however be mentioned, that plastic hinges are only created in the two out of the four side limits of the bearing. The reason is that only in these two sides there are free rods, which are more susceptible to yielding. Compression failure mechanism, similar to that of the unit cell, as this was discussed before, can be identified.

In the case of the shear loading, the plastic hinges are also uniformly distributed in the bearing and the shear failure mechanism can be identified. The creation of the first plastic hinges on the lowest nodes of the cells, as this was identified in Paragraph 3.1 is present in the case of horizontal loading. The combination of vertical and shear loading results in shear and compression failure mechanisms being superimposed. It should be mentioned that more plastic hinges are created on the bearing due to the vertical loading rather than due to the horizontal displacement. This means, that the pentamode bearing could make a great seismic isolation device, since it can successfully absorb horizontal loading, while withstanding a vertical one.

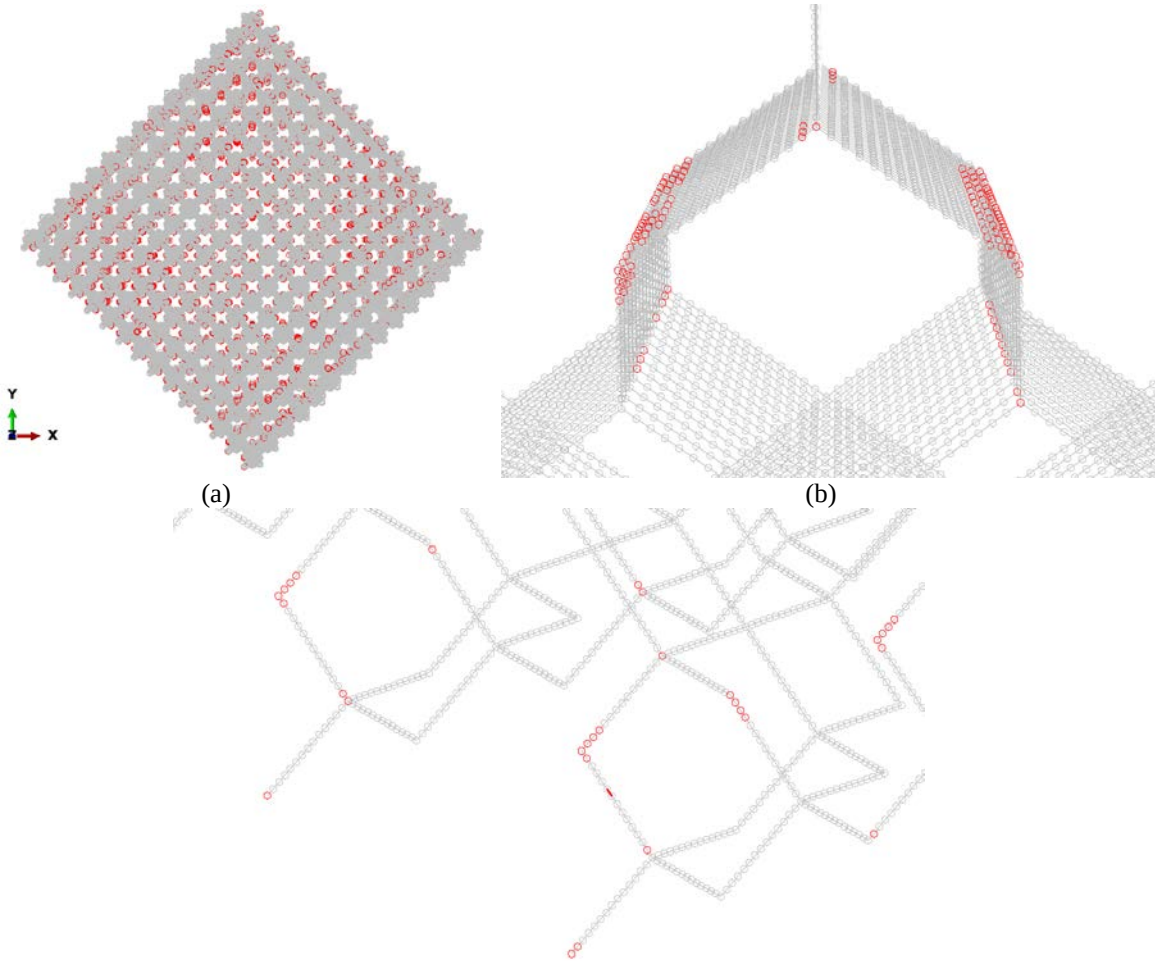

Figure 21. Plastic hinges created on the bearing due to vertical loading, (a) plan view, (b) compression failure mechanism on the top, (c) bottom corner

4. Conclusions

In this work, a bridge bearing composed of layered pentamode modules, is studied. The bearing is constructed by repetitive layers of pentamode unit cells in both the horizontal and vertical axes. A pentamode module is comprised of pentamode unit cells and each cell of intersecting bi-cone rods. The bearing is subjected to a constant vertical load due to the weight of the superstructure as well as to a horizontal shear base load, due to seismic excitation. From the push-over analysis the gradual creation of the plastic hinges reveals the failure mechanisms of the bearing. The pentamode bi-cone rods are modelled via inelastic beam finite elements with an equivalent uniform diameter. The equivalent diameter is calibrated as such to provide the same bending and shear stiffness equal to that of the bi-cone rod. The main conclusions of this study can be summarized as following:

1) The FE stiffness obtained from assuming an equivalent diameter equal to the average of the larger and smaller diameter of the bi-cone rod does not accurately represent the real stiffness parameters of the pentamode structure. This assumption may lead to a deviation from the experimental results of 15% to 880% for the horizontal stiffness and a deviation of 200% - 1900% for the vertical stiffness. The deviation depends on the small and the large diameter of the rod and the slenderness of the formulation.

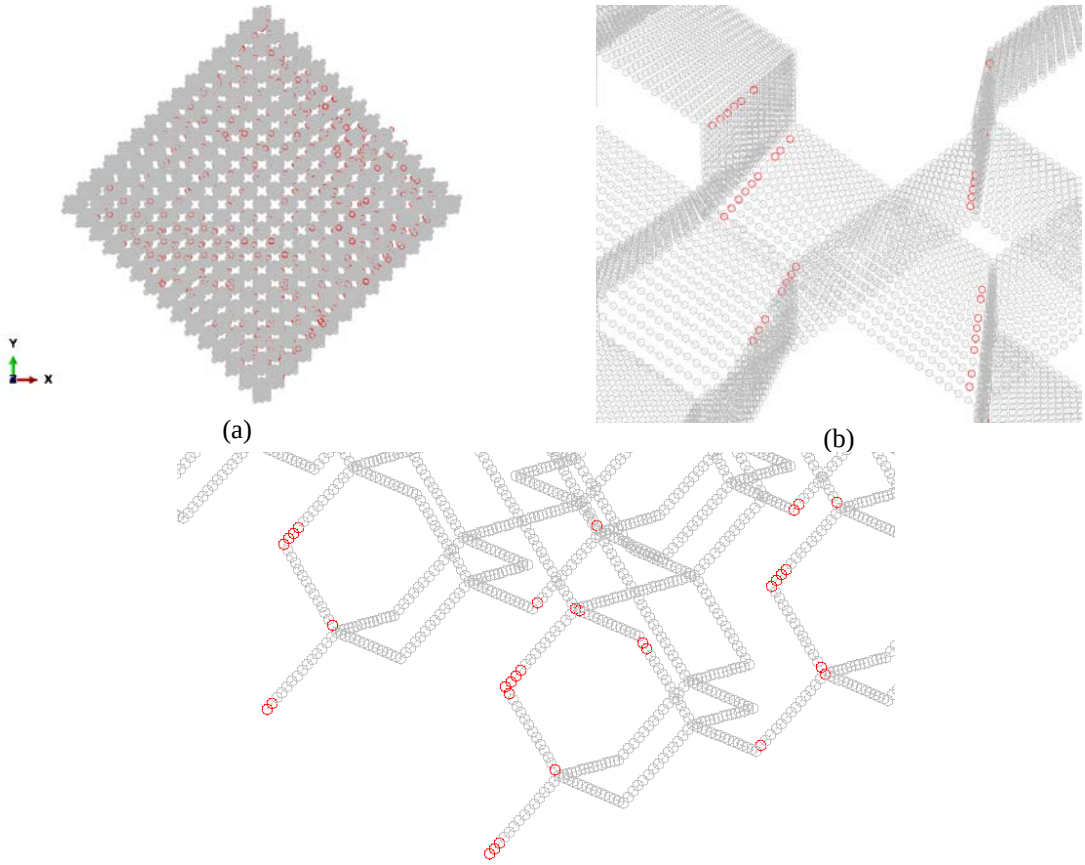

Figure 22. Plastic hinges created on the bearing due to horizontal displacement, (a) plan view, (b) shear failure mechanism, (c) bottom corner

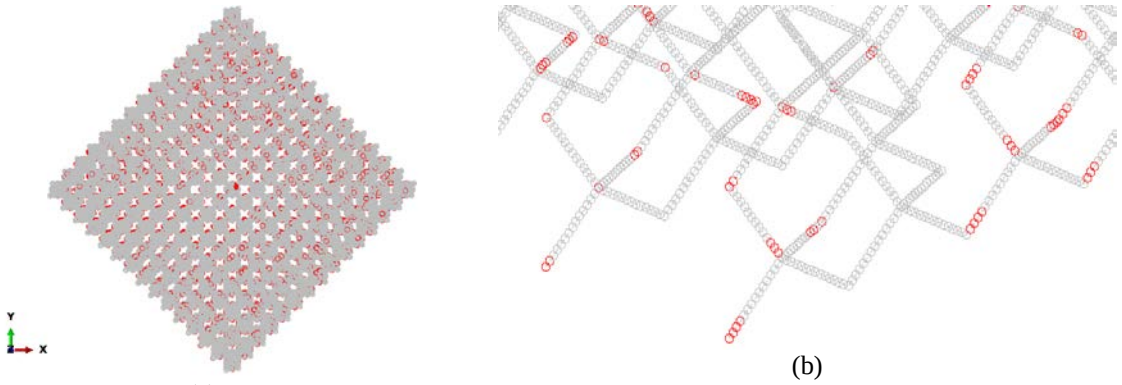

Figure 23. Plastic hinges on elastoplastic formulation under vertical loading & horizontal displacement (a) plan view, (b) bottom corner

2) Therefore, the beam-based modelling could ensure cost-effective simulations without compromising the precision of the results only if an equivalent diameter ensuring a vertical and horizontal stiffness equal to that of the bi-cone rod, would be chosen.

3) For “thick” pentamode structure, the selected equivalent diameter has significant influence on both the vertical and horizontal stiffness. For “slender” pentamode structures, since most of the displacement is attributed to bending, the selected equivalent dimeter is only of moderate importance. To sum up, the slenderer the structure, the greater the importance of the equivalent diameter in the vertical and horizontal stiffness of the structure.

4) The non-linear inelastic response of the pentamode structure significantly varies from the elastic one and thus it must be considered particularly in case of real-life applications.

5) The seismic energy dissipation is attributed to the creation of the plastic hinges at the rod-rod joint.

6) Plastic hinges created due to vertical and/or horizontal loading are homogeneously distributed on the pentamode bearing. The free rods on the two side limits of the bearing are more susceptible to yielding than the constrained rods on the other two side limits.

7) As shown from real-life examples the failure mechanisms of a pentamode unit cell and a pentamode bearing are different in the cases of shear and compression loading.

8) The first plastic hinges on a unit cell under horizontal loading are created on its lower nodes. Similarly, the first hinges on a bearing under shear loading are created on the lowest nodes of the cells comprising it. Shear failure mechanism could be identified in this case.

9) On the contrary, in an elastoplastic unit cell under vertical loading plastic hinges seem to be created simultaneously at its upper nodes, its lower nodes and its central node. Similarly, on the pentamode bearing under compression loading, plastic hinges start to be created in all the rods of the unit cells.

10) From the real-life example studied herein, it is concluded that the pentamode bearing features sufficient shear and compression stiffness to withstand the real-scale induced shear base and can thus be characterized as seismic-isolation device.

5. References

[1] Liu XN, Hu GK, Huang GL, Sun CT. An elastic metamaterial with simultaneously negative mass density and bulk modulus. Applied Physics Letters. 2011;98(25). doi:10.1063/1.3597651

[2] Kapasakalis KA, Antoniadis IA, Sapountzakis EJ, Kampitsis AE. Vibration Mitigation of Wind Turbine Towers Using Negative Stiffness Absorbers. Journal of Civil Engineering and Construction. 2021;10(3):123–139. doi:10.32732/jcec.2021.10.3.123

[3] Chen Y, Liu X, Hu G. Influences of imperfectness and inner constraints on an acoustic cloak with unideal pentamode materials. Journal of Sound and Vibration. 2019;458:62–73. https://doi.org/10.1016/j.jsv.2019.06.005.

[4] Li Q, Zhang M. Composite hexagonal pentamode acoustic metamaterials with tailored properties. Journal of Physics: Condensed Matter. 2020;32:475701.

[5] Kadic M, Bückmann T, Schittny R, Gumbsch P, Wegener M. Pentamode metamaterials with independently tailored bulk modulus and mass density. Physical Review Applied. 2014;2(5). doi:10.1103/PhysRevApplied.2.054007

[6] Milton W. Graeme, Cherkaev V. Andrej. Which elasticity tensors are realizable. Journal of Engineering Materials and Technology. 1995;117(4):483–493. https://doi.org/10.1115/1.2804743

[7] Kadic M, Bückmann T, Stenger N, Thiel M, Wegener M. On the feasibility of pentamode mechanical metamaterials. 2012.

[8] Lumpe TS, Stankovic T. Exploring the property space of periodic cellular structures based on crystal networks. 2021;118(7):2003504118. doi:10.1073/pnas.2003504118/-/DCSupplemental

[9] Xu S, Shen J, Zhou S, Huang X, Xie YM. Design of lattice structures with controlled anisotropy. Materials and Design. 2016;93:443–447. doi:10.1016/j.matdes.2016.01.007

[10] Huang Y, Zhang X, Kadic M, Liang G. Stiffer, stronger and centrosymmetrical class of pentamodal mechanical metamaterialss. Materials. 2019;12(21). doi:10.3390/ma12213470

[11] Li Z, Luo Z, Zhang L-C, Wang C-H. Topological design of pentamode lattice metamaterials using a ground structure method. Materials & Design. 2021;202:109523. https://doi.org/10.1016/j.matdes.2021.109523.

[12] Wu S, Luo Z, Li Z, Liu S, Zhang LC. Topological design of pentamode metamaterials with additive manufacturing. Computer Methods in Applied Mechanics and Engineering. 2021;377. doi:10.1016/j.cma.2021.113708

[13] Fabbrocino F, Amendola A, Benzoni G, Fraternali F. Seismic application of pentamode lattices. Ingegneria Sismica. 2016;33(1–2):62–70.

[14] Fraternali F, Carpentieri G, Montuori R, Amendola A, Benzoni G. On the use of mechanical metamaterials for innovative seismic isolation systems. In: Proceedings of the 5th International Conference on Computational Methods in Structural Dynamics and Earthquake Engineering (COMPDYN 2015). Athens: Institute of Structural Analysis and Antiseismic Research School of Civil Engineering National Technical University of Athens (NTUA) Greece; 2015. p. 349–358. http://www.eccomasproceedia.org/conferences/thematic-conferences/compdyn-2015/3401. doi:10.7712/120115.3401.636

[15] Amendola A, Smith CJ, Goodall R, Auricchio F, Feo L, Benzoni G, Fraternali F. Experimental response of additively manufactured metallic pentamode materials confined between stiffening plates. Composite Structures. 2016;142:254–262. doi:10.1016/j.compstruct.2016.01.091

[16] Amendola A, Carpentieri G, Feo L, Fraternali F. Bending dominated response of layered mechanical metamaterials alternating pentamode lattices and confinement plates. Composite Structures. 2016;157:71–77. doi:10.1016/j.compstruct.2016.07.031

[17] Fraternali F, Amendola A. Mechanical modeling of innovative metamaterials alternating pentamode lattices and confinement plates. Journal of the Mechanics and Physics of Solids. 2017;99:259–271. doi:10.1016/j.jmps.2016.11.010
[18] Amendola A, Benzoni G, Fraternali F. Non-linear elastic response of layered structures, alternating pentamode lattices and confinement plates. Composites Part B: Engineering. 2017;115:117–123. doi:10.1016/j.compositesb.2016.10.027
[19] Smith M. Abaqus/Standard User's Manual, Version 6.9. 2009.